Engineering Poly(ethylene- co -1-butene) through Modulating the Active Species by Alkylaluminum

Yue Yu, Timothy Mckenna, Christophe Boisson, Márcia Lacerda Miranda, Olavo Martins

Engineering Poly(ethylene-*co*-1-butene) Through Modulating the Active Species by Alkylaluminum

Yue Yu,[†] *Timothy F. L. McKenna,*[†] *Christophe Boisson,*[*,†] *Márcia S. Lacerda Miranda*[*,‡] *and Olavo Martins Jr.*[‡]

[†] Univ Lyon, Université Claude Bernard Lyon 1, CPE Lyon, CNRS UMR 5265, Laboratoire Chimie, Catalyse, Polymères et Procédés (C2P2), Bat 308F, 43 Bd du 11 Novembre 1918, F-69616 Villeurbanne, France.

[‡]Braskem SA, Global Catalysis, I&T E&P, 95853-000, Triunfo, Brazil.

ABSTRACT: A $SiO_2/MgCl_2$-bisupported Ziegler-Natta type catalyst is studied in gas phase ethylene/1-butene copolymerization. With a minimal amount of alkylaluminum required to activate the catalyst, polymerization kinetics is profoundly affected by the dosage of it. High dosage of alkylaluminum retards the polymerization but does not kill the catalyst. Through a comprehensive characterization on the samples by DSC, CEF, TGIC, CFC and NMR, it has been showed that alkylaluminum also alters the short chain branching distribution (SCBD) of the copolymer but barely affects the total comonomer incorporation. It is proposed that alkylaluminum alters the active species from producing statistical copolymer chains to producing block polymer chains with C4-enriched and C4-scattered segments. It provides an example of bimetallic structure of active species as well as an approach to tailoring SCBD between statistical copolymer and block copolymer bearing C4-enriched and C4-scattered segments.

KEYWORDS: active sites, alkylaluminum effect, alkyl titanate, bimetallic, monometallic, olefin block copolymer (OBC), Ziegler-Natta catalysis

INTRODUCTION

Alkylaluminum (including derivatives such as Et_2AlCl and $EtAlCl_2$) is commonly employed as a cocatalyst in catalyzed olefin polymerization. Meanwhile, it often plays more than just one role as the activator. For example, it has been clearly recognized that alkylaluminum can bind to the transition metal species in a number of molecular systems and under some circumstances participates in chain growth reaction.[1-12] However, on the classic Ziegler-Natta catalyst (ZNC) a debate around the monometallic or bimetallic mechanism, which argues about the involvement of aluminum species in constructing the active sites, has been lasting for almost as long as its history. In 1962, Cossee proposed a monometallic model based on the crystal structure of α-$TiCl_3$ to account for the steric control during propylene polymerization.[13] A few years later, Rodriguez et al. proposed a bimetallic model to explain the impact of alkylating agents on stereospecificity of $TiCl_3$ catalysts.[14] Thereafter Corradini[15-16], Busico[17] and Sacchi[18] et al. solidified the credibility of monometallic mechanism. In the work of Sacchi, an isotope-labeling approach was employed to study the stereocontrol of the first insertion and provided strong evidences for monometallic mechanism. On the other hand, Doi[19-20], Xu[21] and Terano[22] found more evidences for the bimetallic mechanism based on polypropylene microstructural analysis. From the point of view of catalyst itself, the clear presence of aluminum species on the catalyst surface has demonstrated the capability of alkylaluminum to form complexes with catalyst components.[23-25] Recently, Chiesa, Groppo and their colleagues through advanced electron paramagnetic resonance (EPR)

methods indirectly observed the aluminum species in the proximity of titanium in an industrial fourth-generation ZNC[26] and thereafter recorded a direct Fermi contact between Ti(III) and Al via chlorine bridge in a model catalyst[27].

Besides the controversial roles of aluminum species raised from the context of steric control, its roles in comonomer incorporation have not attracted as much attention. What is known as the fact is that employing different alkylaluminums could impact the copolymer composition not only in soluble molecular catalyst systems[28-31], but also in supported Ziegler-Natta-type ones[32-37]. Noteworthily, the US patent 8546499 B2 of Borealis AG taught that employing Et_2AlCl instead of Et_3Al during polymerization could produce flat comonomer distribution at the price of slightly decreased overall comonomer incorporation.[36] And employing $EtAlCl_2$ during catalyst preparation could result in similar effects.[37] It is superior to the usual circumstance where ZNCs produce copolymer with decreasing comonomer incorporation over molecular weight (MW),[38-40] because a relatively high degree of comonomer incorporation in the high molecular weight fraction of polyethylene is desired for obtaining high impact toughness and high environmental stress cracking resistance (ESCR).[41-46] Thus it would be as well of industrial interest as of the academic one to better understand the likely involvement of aluminum species into the chain formation, particularly on the comonomer enchainment.

In this study, a $SiO_2/MgCl_2$-bisupported catalyst is studied in gas phase

ethylene/1-butene copolymerization. This paper reports a comprehensive investigation into the effects of alkylaluminum on the kinetics and copolymer chemical composition distribution (CCD). It attempts to shed light on the mechanistic roles of the aluminum species during copolymerization.

EXPERIMENTAL SECTION

Chemicals

A $SiO_2/MgCl_2$-bisupported catalyst prepared according to European patent 1515995 B1 (1.44wt% Ti, 1.45wt% Mg) was kindly donated by Braskem S.A.[47] Triethylaluminium (TEA, from SGS), triisobutylaluminium (TIBA, from Witco) were used as received. Ethylene (purity 99.95%) was purchased from Air Liquide (Paris, France) and passed through three different purification columns before use: a first one filled with reduced BASF R3-16 catalyst (CuO on alumina), a second one filled with molecular sieves (13X, 3A, Sigma-Aldrich), and a last one filled with Selexsorb COS (Alcoa). H_2 (ALPHAGAZ high purity gas) was purchased from Air Liquide and was used as received.

Polymerization procedure

Gas phase polymerization was conducted in a spherical reactor illustrated in **Scheme 1**. The curved agitator was able to vigorously stir the catalyst/polymer particles along with dispersant (thermally treated NaCl grain) to achieve sufficient contact with gas phase. After the reactor was conditioned at 85 ℃ under vacuum for two hours, the reactor was cooled down to room temperature and filled up with argon and 50 g of NaCl grain. A pre-determined amount of neat alkylaluminum was injected. Then the reactor was heated up again. After the temperature in the reactor was stabilized at 85 ℃, 200 mg catalyst (mixed with 20 g NaCl in glovebox and transferred into cartridge) was flushed down to the reactor by pressurized monomer from monomer

reservoir. Immediately the target pressure of monomer was reached and maintained constant (± 0.02 bar). As long as polymerization reaction occurred in the reactor, pressure of the reservoir dropped and was recorded by both computer and manual reading. The time of polymerization was limited so as to keep the conversion of 1-butene below 10%. At the end of reaction, the reactor was depressurized and cooled. Product was retrieved and washed by water and then dried under vacuum at 70 °C.

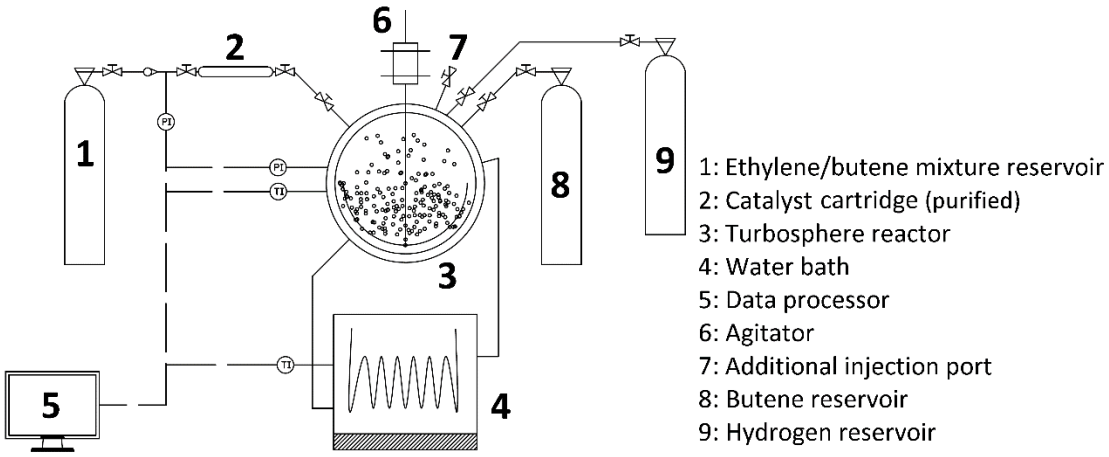

Scheme 1. Diagram of ethylene/butene copolymerization setup. **#to be moved to SI#**

Differential scanning calorimetry (DSC) characterization

DSC analyses were performed with Mettler Toledo DSC 1 system equipped with an auto-sampler and a 120 thermocouple sensor. The temperature and the heat flow of the equipment were calibrated with an indium standard. All samples were accurately weighed (6 ± 0.1 mg) and sealed in aluminium pans. An empty aluminium pan was employed as the reference. Dry nitrogen with a flow rate set at 50 mL min^{-1} was used as the purging gas. The STARe thermal analysis software was used to process the

collected data. Melting peak temperature (T_m) was defined as the temperature corresponding to the melting peak point; the crystallinity (by weight, w_c) of the samples was calculated through $w_c = \Delta H_f/\Delta H_{f0}$, where ΔH_f (J g^{-1}) is the melting enthalpy of the sample and ΔH_{f0} (293 J g^{-1}) is the melting enthalpy of a 100% crystalline polyethylene. Conventional DSC method: Samples were heated to 180 °C to erase thermal history and then cooled to −20 °C before being heated to 180 °C. Heating rate 10 °C min^{-1}, cooling rate −10 °C min^{-1}. Successive self-nucleation/annealing (SSA) DSC measurements were performed by employing two different protocols designed according to the literature[48-50]:

i. Thermal protocol # 1: Samples were heated to 170 °C and held for 5 min to erase the thermal history. The samples were then cooled to 50 °C for crystallization until saturation. The ideal self-nucleation temperature ($T_{s,ideal}$) 125 °C was determined through self-nucleation (SN) experiments (Figure S1). The interval (ΔT_s) between neighboring isothermal crystallization temperatures was 5 °C which generated 15 stages until 55 °C. Each isothermal crystallization step lasted for 5 min. The samples were cooled to 50°C between each two neighboring isothermal crystallization steps. After the last isothermal crystallization step, the samples were cooled to −20 °C and then heated to 170 °C for the measurement scan. For the whole procedure, heating rate 10 °C min^{-1}, cooling rate −10 °C min^{-1}.

ii. Thermal protocol # 2: This is a modified version of protocol #1, made in order to enhance the resolution of SSA-DSC results on the fraction with highest T_m.

The difference from #1 is employing interval (ΔT_s) 2 ℃ and 1 ℃. And the lowest isothermal crystallization temperature was adjusted accordingly due to the time consumption of the experiments. The other parameters were kept the same.

Gel permeation chromatography (GPC) characterization

High temperature GPC analyses were performed using a Viscotek system (from Malvern Instruments) equipped with three columns (PLgel Olexis 300 mm × 7 mm I.D. from Agilent Technologies). 200 μL of sample solutions with a concentration of 5 mg mL^{-1} were eluted in 1,2,4-trichlorobenzene using a flow rate of 1 mL min^{-1} at 150 ℃. The mobile phase was stabilized with 2,6-di-tert-butyl-4-methylphenol (butylated hydroxytoluene, BHT, 200 mg L^{-1}). Online detection was performed with a differential refractive index detector and a dual light scattering detector (LALS and RALS) for absolute molar mass measurement. The OmniSEC 5.02 software was used for calculations.

Chemical composition distribution measurement

GPC-IR

The experiments were conducted with a Polymer Char high temperature gel permeation chromatographer (HT-GPC) at 145 ℃ under 1 mL min^{-1} flow rate of

1,2,4-trichlorobenzene (TCB). The instrument was equipped with an infrared detector that was used as mass and chemical composition detector. The HT-GPC was calibrated with narrow polystyrene standards to measure MWD, and with metallocene ethylene/1-butene copolymers to measure SCBD.

Crystallization elution fractionation (CEF)

CEF characterization was performed on a Polymer Char CEF instrument using a stainless-steel column filled with glass beads. The samples were dissolved in 10 mL vials for 1 h at 150 ℃ with 1,2,4 trichlorobenzene (TCB) containing 300 ppm of BHT and purge with nitrogen. For each entry, 200 μL of sample was injected at a concentration of 0.5 mg mL^{-1} in a volume of 200 μL at 150 ℃. Cooling stage ends at 35 ℃ at a rate of −1 ℃ min^{-1} with flow rate of 0.35 mL min^{-1}. Heating stage ends at 140 ℃ at a rate of 1 ℃ min^{-1} with flow rate of 1 mL min^{-1}.

Thermal gradient interaction chromatography (TGIC)

TGIC characterization was performed on the same Polymer Char CEF instrument but equipped with a Hypercarb column. The samples were dissolved in 10 mL vials for 1 h at 150 ℃ with 1,2,4 trichlorobenzene (TCB) containing 300 ppm of BHT and purge with nitrogen. For each entry, 200 μL of sample was injected at a concentration of 0.5 mg mL^{-1} at 150 ℃. Cooling stage ends at 40 ℃ at a rate of −5 ℃ min^{-1} without flow. Elution begins isothermally at 40 ℃ for 5 min at a flow rate of 0.5 mL min^{-1}. Heating stage ends at 160 ℃ at a rate of 2 ℃ min^{-1} with a flow rate of 0.5 mL min^{-1}.

Cross Fractionation Chromatography (CFC)

CFC characterization combines Temperature Rising Elution Fractionation (TREF) and GPC to provide 3-D bivariate distribution analysis.[51] This correlates MWD and chemical composition distribution (CCD). TREF×GPC cross fractionation was performed using a cross-fractionation chromatography (CFC) instrument provided by Polymer Char (Spain). 1,2-Dichlorobenzene (*o*-DCB), with 0.1 ppm of antioxidant butylated hydroxy toluene (BHT), was used as solvent for sample dissolution and analysis. For each run, 0.5 mL of polymer solution (3.5-3.6 mg mL^{-1}) was loaded into the TREF column. During the crystallization step, a cooling rate of 0.5 °C min^{-1} was used. During the elution step, the temperature was increased from 30 to 140 °C with a stepwise temperature increase of 3 °C. An IR5 MCT infrared detector was used for CCD measurement. The elution temperature range of 30 °C to 140 °C was divided into 20 to 25 fractions. For GPC analysis, a flow rate of 1 mL min^{-1} and 3× PLGel 10 micron mixed columns (Polymer Laboratories Inc.) were used. Narrow polystyrene standards were employed to calibrate GPC measurement.

Nuclear magnetic resonance spectroscopy (NMR) characterization

For each sample, polymer was dissolved in a mixture of benzene-d_6/tetrachloroethylene (C_6D_6/TCE, 1/2 volume ratio) under heating with concentration 75 mg mL^{-1} in a 10 mm tube. The spectra were recorded with a Bruker AVANCE II spectrometer operating at 100.6 MHz for ^{13}C (400 MHz for ^{1}H) at 90 °C. ^{1}H spectra were recorded under the following operating conditions: zg30 sequence,

acquisition time 4.09 s, relaxation delay 3 s, 400 scans. ^{13}C spectra were recorded under the following operating conditions: zgig70 sequence (without nuclear Overhauser effect), acquisition time 1.36 s, relaxation delay 10 s, 2000 scans. Residual proton (δ 7.15 ppm) of benzene and backbone carbon $S_{\delta+\delta+}$ (δ 29.58 ppm) of polyethylene were used as internal reference for ^{1}H and ^{13}C NMR spectra, respectively. ^{1}H NMR signals of unsaturated chain ends were assigned according to literature.[52-54] Copolymer composition was calculated according to Randall's method.[55]

RESULTS AND DISCUSSION

Polymerization kinetics

The catalytic system employed in this study requires a minimum amount of alkylaluminum to be fully activated (molar ratio of Al over Ti or briefly *r*Al,Ti needs to be between 6 and 12, Figure 1). It suggests that a function of alkylaluminum is to form active species. The kinetics show early decay at low level of TEA dosage, displaying the role of TEA as the scavenger. On the other hand, a high dosage of TEA results in decreased activity with a prolonged build-up stage during which the activity keeps increasing. Unlike the effects to classic ZNCs (where high dosage of TEA usually results in decreased activity and fast activity decay)[56-58] but similar to the effects to some metallocenes (which are hindered instead)[59-61], a very high dosage of TEA (7.2 mmol, *r*Al,Ti = 120) does not kill the catalyst in the time span of this study (up to 220 min) but allows a gradual growth of activity (Figure 2). This copolymerization system shows an enhancement in activity upon addition of H_2 (Figure 3) particularly at low *r*Al,Ti. It seemingly implies a dormant phenomenon caused by 1-butene.

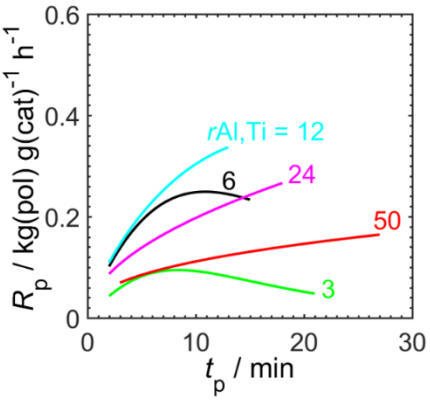

Figure 1. Effects of dosage of TEA on kinetics. *r*Al,Ti = 3, 6, 12, 24 and 50 correspond to TEA dosage 0.36 mmol (doubled amount of catalyst), 0.36 mmol, 0.72 mmol, 1.46 mmol and 2.93 mmol, respectively. C4/(C2+C4) = 33%. P_{C2}= 4 bar, P_{C4}= 2 bar, P_{H2} = 0.76 bar.

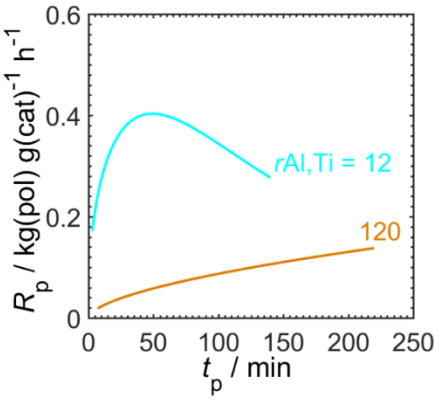

Figure 2. Kinetics shows the impact of very high TEA dosage. *r*Al,Ti = 12 and 120 correspond to TEA dosage 0.72 mmol and 7.2 mmol (~ 1 mL neat form in 2.5 L reactor), respectively. C4/(C2+C4) = 20%. P_{C2}= 4 bar, P_{C4}= 1 bar, P_{H2} = 0.76 bar.

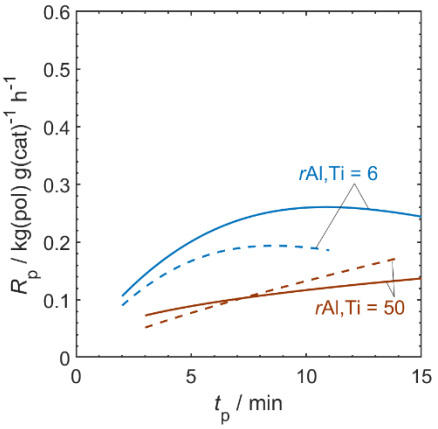

Figure 3. Effects of H_2 and dosage of TEA on kinetics. (Solid lines) with H_2, (dashed lines) without H_2. P_{C2}= 4 bar, P_{C4}= 2 bar, P_{H2} = 0.76 bar (if applicable).

Melting behaviors of copolymer

C2/C4 copolymer samples prepared with two different gas compositions (20% and 33% C4 in monomer gas mixture) and various Al/Ti ratio (*r*Al,Ti) are characterized by DSC and NMR. The DSC traces of the first and second heating scan can be found in Figure S2-S5. The results of the 2nd scan are summarized (Table 1 and Figure 4) and discussed in this section.

In the presence of H_2, both T_m and w_c slightly increase over Al/Ti ratio (*r*Al,Ti). T_m is independent of the C4 content in copolymer ([C4]). For example, when *r*Al,Ti = 12 (TEA) stays the same, the increased [C4] in copolymer (with C4 in the gas phase increased from 20% to 33%) from 4.56 mol% to 8.77 mol% results in the decreased crystalline fraction from 45% to 32% whereas T_m, which is determined by the length of dominant crystallizable segments (successive ethylene sequence), stays at 122.8 ℃. On the other hand, when the gas composition is kept at C4/(C2+C4) = 20%, the increased *r*Al,Ti (TEA) causes an increase in crystallinity from 42% to 48% while the [C4] was marginally affected. So it clearly indicates that alkylaluminum does not only determine the length of the successive ethylene sequence of polymer in the crystalline fraction, but also alters the proportion of the crystalline and amorphous fractions. It is marked that TEA and TIBA show basically the same effects, indicating the difference in alkyl is not significant in this case.

In the absence of H_2, both the T_m and w_c of copolymer are lower than that prepared in

the presence of H_2 although the [C4] is very similar. And the trends of them increasing over *r*Al,Ti is more clearly demonstrated compared to the case in the presence H_2. The overall [C4], again, is not significantly affected by *r*Al,Ti.

Table 1. DSC (2nd heating) and GPC results of LLDPE along with the corresponding C4 incorporation.

Cond.[a]	*r*Al,Ti	T_m/ ℃	w_c/ %	*M*n/ kDa	*M*w/ kDa	*Đ*	C4 incorp.[b] /mol%
TEA 20% C4/(C2+C4)	3	122.67	41.81	31	109	3.5	3.46
	6	122.60	45.03	27	103	3.8	-
	12	122.82	45.54				4.56
	24	123.95	48.88	8	73	9.1	-
	50	124.25	47.61	6	59	9.8	3.60
TIBA 20% C4/(C2+C4)	6	122.32	45.22	52	156	3.0	3.56
	12	122.72	46.03				4.09
	50	123.81	47.46	10	83	8.3	3.11
TEA 33% C4/(C2+C4)	3	120.85	32.29	45	143	3.2	6.25
	6	121.62	32.46	21	94	4.4	7.42
	12	122.75	32.14				8.77
	24	123.79	38.13	5	69	13.8	6.60
	50	124.03	35.69	4	45	11.2	7.47
TIBA 33% C4/(C2+C4)	6	120.55	34.72	26	92	3.5	-
	12	122.59	34.45				7.79
	50	123.54	37.21	7	62	8.9	6.27
TEA 33% C4/(C2+C4) without H_2	6	112.28	26.33	236	489	2.1	6.56
	12	114.06	26.95				7.16
	24	116.20	29.15	11	225	20.5	7.39
	50	118.81	32.78	4	117	29.2	7.71

[a] Cocatalyst and gas composition (P_{C2}= 4 bar, P_{H2} = 0.76 bar if not specified).
[b] C4 incorporation measured by NMR.

GPC results show that increased dosage of alkylaluminum results in decreased MW as an unambiguous evidence of chain transfer effect. Meanwhile the dispersity *Đ* significantly grows. GPC profiles can be found in Figure S6-S8.

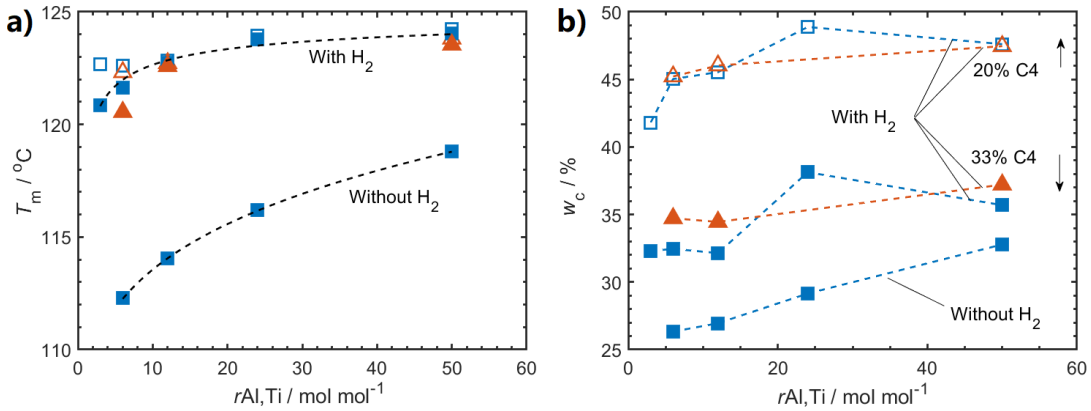

Figure 4. The influences of type of alkylaluminum (TEA and TIBA) and Al/Ti ratio (*r*Al,Ti) on **a**) melting temperature (T_m) and **b**) crystallinity (w_c). (Squares) TEA, (triangles) TIBA. (Open markers) C4/(C2+C4) = 20%, (full markers) C4/(C2+C4) = 33%. P_{C2}= 4 bar, P_{H2} = 0.76 bar if applicable.

Thermal fractionation of copolymer by SSA DSC is based on the principle that the lamellae thickness is correlated with the length of successive ethylene sequence.[50, 62-65] The results at ΔT_s = 5 °C in Figure 5a show that the increasing *r*Al,Ti results in higher content of the fraction with high T_m (or long ethylene sequence). Meanwhile the fractions with low T_m are very similar. Fractionation of the portion with the highest T_m at higher resolution (ΔT_s = 2 °C and 1 °C in Figure 5b and 5c, respectively) demonstrates that the increasing fraction with high T_m is contributed by the emerging fraction with long ethylene sequence. Different from alkylaluminum mostly affecting the fraction with high T_m, H_2 promotes the production of ethylene sequences with all lengths.

In summary, the results of DSC analysis suggest that the dominant factor for the length of the crystallizable segments of the polymer is the availability of AlR_3 and H_2 rather than 1-butene.

#Figure 5 has been updated#

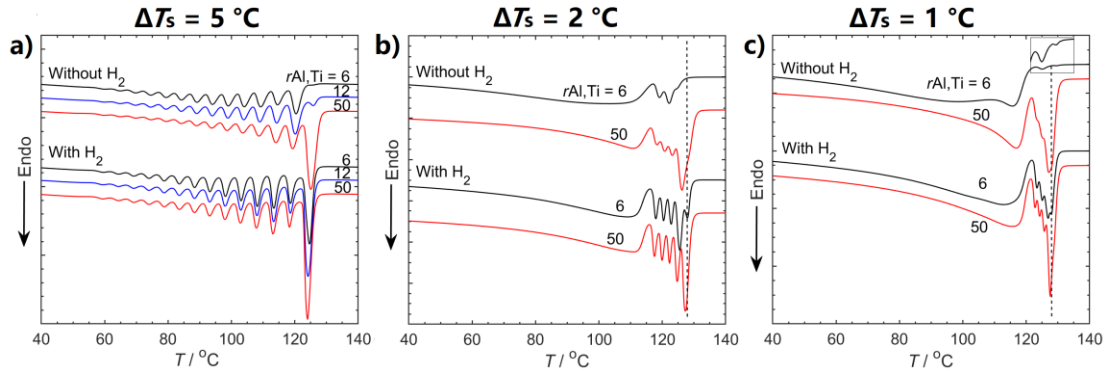

Figure 5. Successive self-nucleation/annealing (SSA) DSC endotherms of C2/C4 copolymer (6 ± 0.1 mg), demonstrating the effects of *r*Al,Ti (TEA). **a**) thermal protocol # 1 with ΔT_s = 5 ℃, **b**) thermal protocol # 2 with ΔT_s = 2 ℃, **c**) thermal protocol # 2 with ΔT_s = 1 ℃. P_{C2}= 4 bar, P_{C4}= 2 bar, P_{H2} = 0.76 bar (if applicable). The dashed lines in b) and c) are eye's guide for T_m of the peak. The inset in c) is amplification of the corresponding part of the curve.

Chemical composition distribution (CCD) of copolymer

GPC-IR

In Figure 6 typical GPC spectra of copolymer in this study are illustrated with SCBD over MW. The samples show decreasing comonomer incorporation over MW which is similar to typical ZNC systems.[38-40] ~~In the following part we will discuss about the origin of this feature.~~

#Figure 6 has been updated#

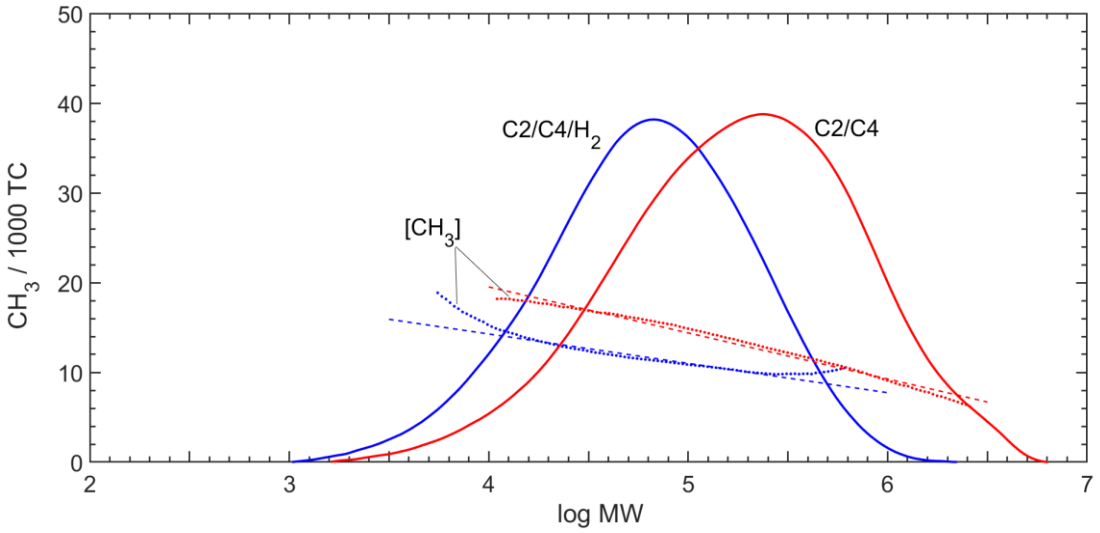

Figure 6. Typical GPC profiles of copolymer with the data of SCBD over the MW prepared at *r*Al,Ti = 12. P_{C2}= 4 bar, P_{C4}= 1 bar, P_{H2} = 0.76 bar (if applicable). Fitted correlation between [CH_3] and logMW: without H_2, [CH_3] = -5.13 logMW + 40.04; and with H_2, [CH_3] = -3.27 logMW + 27.37. TC means Total Carbon.

One-Dimensional Fractionation

Four samples of C2/C4 copolymer prepared with TEA as cocatalyst ([*r*Al,Ti = 6, *r*Al,Ti = 50] × [with H_2, without H_2]) were comparatively characterized by CEF and TGIC; and the results are demonstrated in Figure 7 to show the effects of *r*Al,Ti and H_2 on the CCD of the copolymer.

CEF is a method based on the crystallizability of the sample fractions.[66-67] The results show significant presence of room temperature-soluble fraction (RTSol) and crystalline part. The latter one consists of two major components: one with higher T_e ($CRYS_{HTe}$) and the other with lower T_e ($CRYS_{LTe}$). Comparing the two samples prepared without H_2 (brown lines in Figure 7), it is showed that higher *r*Al,Ti unambiguously gives rise to a higher T_e of the most crystalline peak. It indicates that the length of the longest ethylene sequence (which is the determining factor of T_e in crystallization-based solvent fractionation[68]) increases upon higher dosage of alkylaluminum. The results also demonstrate that higher *r*Al,Ti causes a significant decrease in the medium-T_e fraction and an increase in RTSol. It seems to agree with the SSA DSC analysis which suggests that the chemical composition of the copolymer becomes more heterogeneous in composition upon increased *r*Al,Ti (C4-poor fraction becoming poorer and C4-rich fraction becoming richer). The influence of *r*Al,Ti diminishes in the presence of H_2.

TGIC is a chromatography exploiting the interaction between polymer chains and the graphitic stationary phase.[69-76] Above a critical value of chain length, the elution temperature (T_e) is almost independent of MW but dependent on the average length of the ethylene sequence for an ethylene/α-olefin random copolymer and on the total length of the ethylene sequence for a block copolymer.[69, 74] Generally we reach the same conclusion as in CEF part: more heterogeneous composition is obtained at high

*r*Al,Ti. Besides that, it shows that the two samples prepared without H_2 have clearly higher end T_e compared to the counterparts with H_2. It is reproducible because Figure 7 and Figure S10 are based on two batches of characterization, respectively. This is probably caused by the high MW in the absence of H_2 (Figure S8) which slightly enhances the adsorption on graphite surface. Apparently the chain transfer (CT) to H_2 occurs to all the chains indiscriminately while CT to alkylaluminum has different preferences for chains. It is better demonstrated in the cross fractionation as follows.

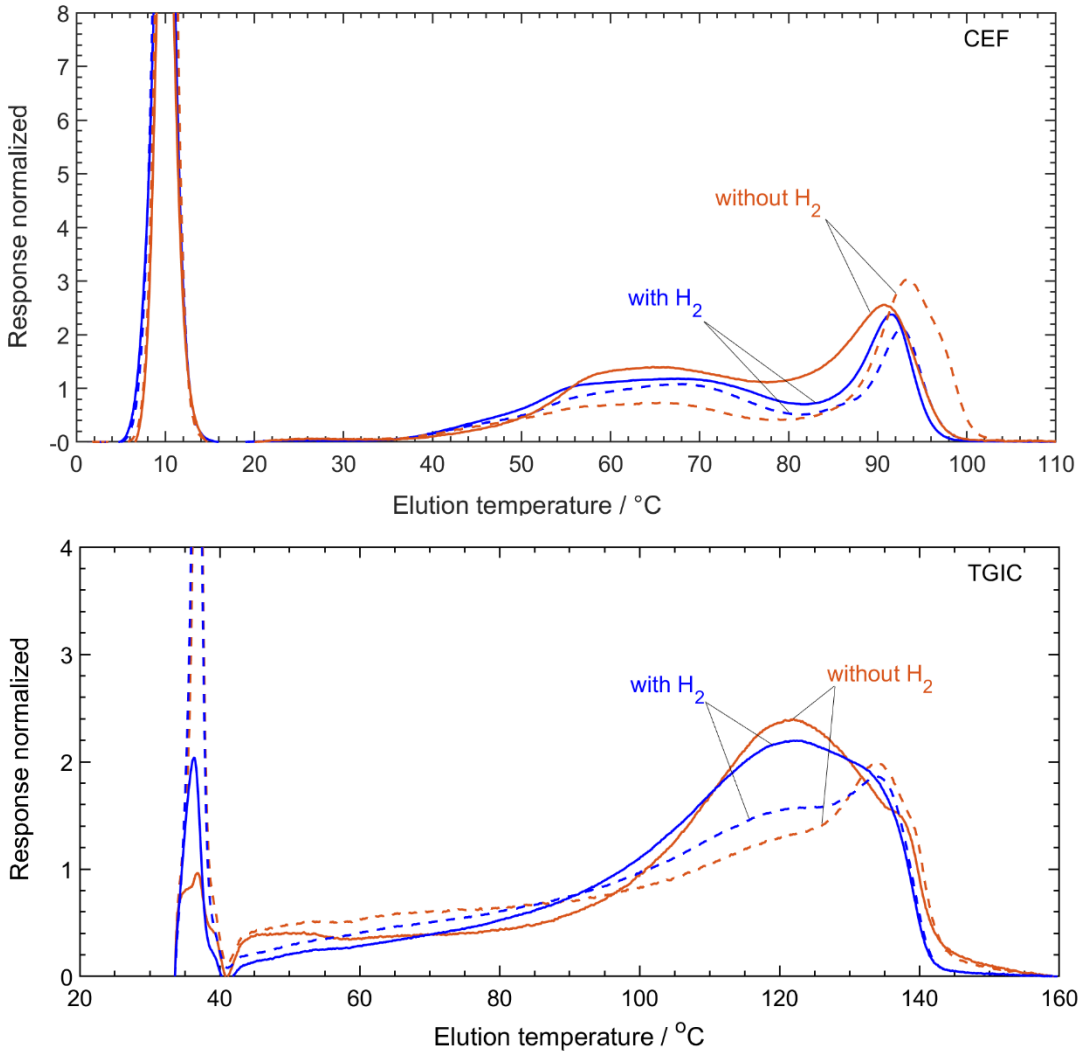

Figure 7. CEF and TGIC (with qualitative SCBD) profiles of C2/C4 copolymer samples showing the effects of *r*Al,Ti (TEA) and H_2 (presence and absence of H_2 during polymerization). (Solid lines) *r*Al,Ti = 6, (dashed lines) *r*Al,Ti = 50. Area under each curve was normalized. P_{C2}= 4 bar, P_{C4}= 2 bar (33% C4), P_{H2} = 0.76 bar (if

applicable). CEF RTSol: 33.15% (without H_2, *r*Al,Ti = 6), 48.97% (without H_2, *r*Al,Ti = 50), 44.51% (with H_2, *r*Al,Ti = 6), 52.64% (with H_2, *r*Al,Ti = 50).

Cross-Fractionation

Three ethylene/1-butene copolymer samples prepared with gas phase containing 33% of C4/(C4+C2) are characterized by CFC: a) without H_2, *r*Al,Ti = 6; b) without H_2, *r*Al,Ti = 50; c) with H_2, *r*Al,Ti = 6. TEA is the cocatalyst.

CFC characterization is conducted in two dimensions: elution temperature and molecular weight. The samples are fractionated with TREF firstly; and then each fraction is characterized by GPC automatically. TREF data are demonstrated in Figure 8.

It is not surprising that the shape of TREF profiles is very similar to CEF (Figure 7) because both of them are based on crystallization/dissolution process. However, there exist two major differences: 1) the samples (particularly the one prepared without H_2 at *r*Al,Ti = 6) show rather flat [C4] over T_e by TREF compared to by CEF (Figure 8 and Figure S10); 2) TREF gives lower content of RTSol than CEF does. It is known CEF has reduced cocrystallization effect compared to TREF.[66] The differences suggest part of the C4-rich fraction (soluble at room temperature) cocrystallizes with the crystalline fraction in TREF. In this case of scenario, it likely further suggests that at least part of the RTSol has blocky characteristics because: 1) it requires long ethylene sequence in the structure to cocrystallize and 2) it is not possible for C4-rich chains to form long ethylene sequence if the comonomer units distribute in a statistically random manner.[74] The *n*-pentane (b.p. 36 ℃) extracted fraction of a

selected sample (Figure S11) demonstrates exceptionally high content of sequences BEEE (conjunction of segments) and EBEB (soft segment), and therefore seemingly supports this possibility. Since the relative difference in the RTSol (between CEF and TREF) is less for the cases with higher *r*Al,Ti or in the presence of H_2, i.e. less cocrystallization, it suggests that increasing *r*Al,Ti or adding H_2 reduces the blocky characteristics of the copolymer. And it is also reflected by the decreasing [C4] over T_e which is typical for random copolymer. It may be attributed to the chain transfer to TEA or to H_2 that 'cuts' the growing block copolymer into C4-rich and C4-poor polymer chains. The resulting C4-rich chains join the low MW fraction in the RTSol and cause significant increase in [C4] at low MW side as being demonstrated in the inset of Figure 8.

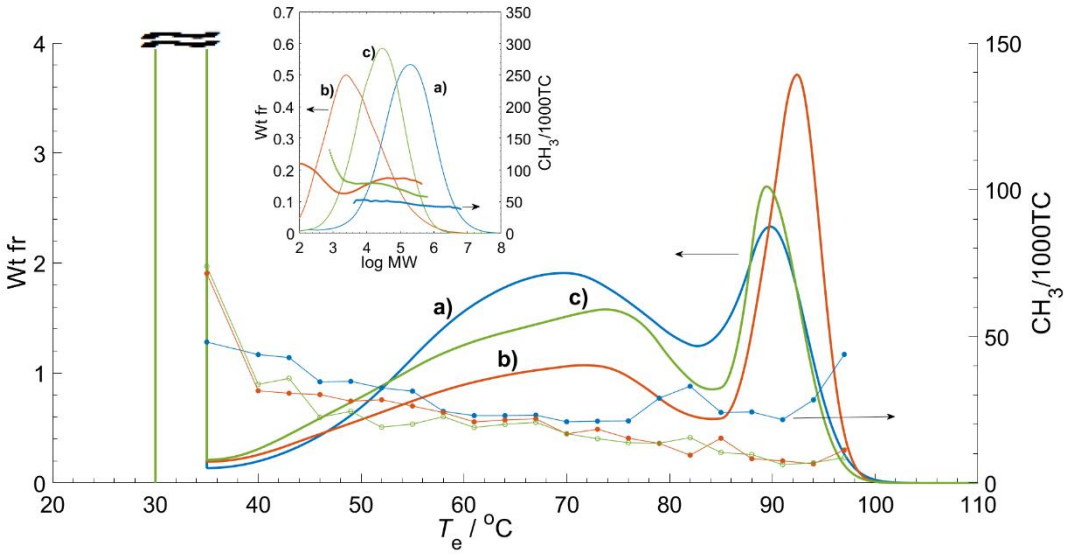

Figure 8. TREF profiles with SCBD measured by CFC instrument. P_{C2}= 4 bar, P_{C4}= 2 bar, P_{H2} = 0.76 bar (if applicable), TEA as cocatalyst. **a**) Without H_2, *r*Al,Ti = 6; **b**) without H_2, *r*Al,Ti = 50; **c**) with H_2, *r*Al,Ti = 6. The weight percentage of the RTSol (30 °C<T_e<35 °C) is 23.14%, 38.36% and 33.99%, respectively. The inset is the GPC-IR data of the RTSol. CH_3 content has been corrected with NMR data of overall C4 incorporation.

3D maps (TREF-GPC) of the crystalline fraction are showed in Figure 9. The results confirm that the crystalline part of copolymers consists of two major components: one with higher T_e ($CRYS_{HTe}$) and the other with lower T_e ($CRYS_{LTe}$). Interestingly the two components have very similar MWD to each other and to RTSol (inset of Figure 8) at low *r*Al,Ti in the absence of H_2 (sample a). Increasing *r*Al,Ti does not significantly affect the MWD of $CRYS_{HTe}$ but causes a decrease in MW for $CRYS_{LTe}$ (sample b). H_2 decreases the MW and dispersity of all fractions (sample c).

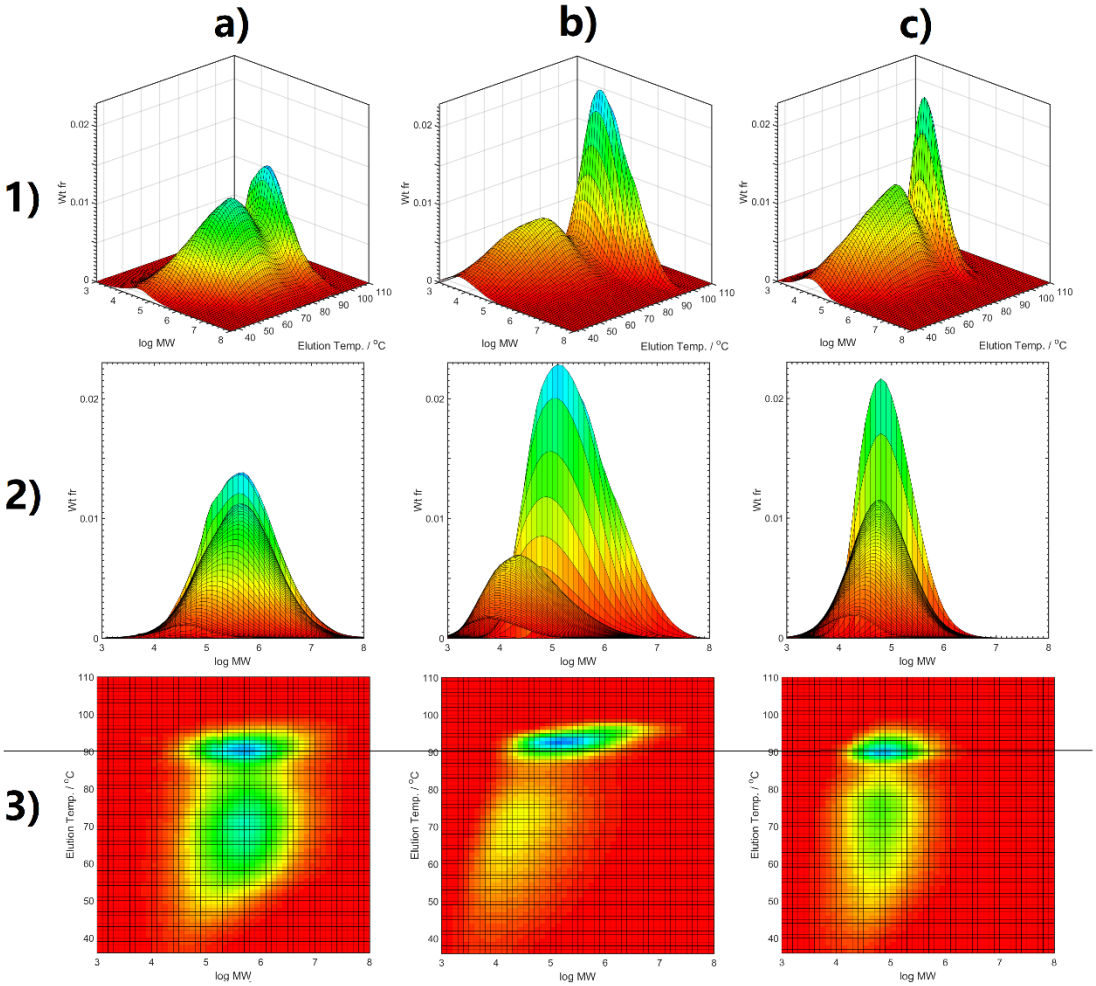

Figure 9. 3D profiles and 2D projections of CFC results excluding RTSol. 1) 3D profiles; 2) 2D projections of weight fraction distribution/molecular weight; 3) 2D projections of elution temperature/molecular weight. P_{C2}= 4 bar, P_{C4}= 2 bar, P_{H2} = 0.76 bar (if applicable). a) Without H_2, *r*Al,Ti = 6; b) without H_2, *r*Al,Ti = 50; c) with H_2, *r*Al,Ti = 6. The weight percentage of $CRYS_{LTe}$ (T_e = 40-85 ℃) and $CRYS_{HTe}$ (T_e =

88-97 ℃) are: a) 57.27% and 19.57%; b) 35.26% and 26.39%; c) 50.35% and 15.66%, respectively. The line in 3) is eye's guide for T_e of $CRYS_{HTe}$ peak.

GPC-IR characterization on the elution fractions of TREF reveals how [C4] distributes across the fractions of the copolymer (Figure 10-3). First of all, for all samples it is found that: 1) dispersity of each elution fraction (Table S1 and Figure S12) is much higher than Flory component ($Đ$ = 2) and 2) almost each fraction has higher [C4] at lower MW. It indicates that multiple components are still mixed and the fractionation is not complete. It supports the presence of cocrystallization aforementioned. Secondly, comonomer distribution pattern of $CRYS_{LTe}$ is distinct from $CRYS_{HTe}$. It suggests these two components with different length of the longest crystallizable segments are generated by different families of active species. Thirdly, some fractions of $CRYS_{HTe}$ have surprisingly high [C4] which has almost made butene units the majority in some of the chains by judging from the CH_3 counting (150 CH_3 per 1000 TC gives 43 mol% of butene incorporation) and clearly cannot be explained if the copolymer is statistically random. The copolymer has to have some extent of blocky characteristics.

The next question is how blocky the copolymer is or how much in the total chains the block ones occupy. We believe it can be qualitatively evaluated based on the effects of chain transfer agents. Either employing TEA or H_2 as the chain transfer agent, only the [C4] at low MW is significantly reduced. It reflects the process where the soft segments concentrated with butene units are cut off and elute as part of the RTSol. The results suggest that the block chains are at least contained in the low MW fractions.

The change in composition at higher dosage of alkylaluminum is believed to gain contribution from the change of nature of active species as well. It is backed by two evidences: 1) higher *r*Al,Ti results in an increase in the weight percentage of $CRYS_{HTe}$ (caption of Figure 9) suggesting against a pure loss in the chain segments; 2) peak T_e of both $CRYS_{LTe}$ and $CRYS_{HTe}$ slightly increases at higher *r*Al,Ti indicating a change in the length of the longest crystallizable segments (Figure 8).

The low intensity of the peak with the highest T_m in SSA DSC for sample a (*r*Al,Ti = 6, without H_2 in Figure 5) is not reflected in TREF analysis. It persists with long duration of isothermal crystallization up to 60 min (Figure S13). The difference between SSA DSC and TREF reflects the blocky characteristics of the sample a. In TREF the ethylene sequences anchor the whole block chains on the filler until the temperature reaches the corresponding T_e of the sequence. However they do not generate significant heat effect for DSC analysis due to their minor portion. That is why they show intenser presence with TREF than with DSC.

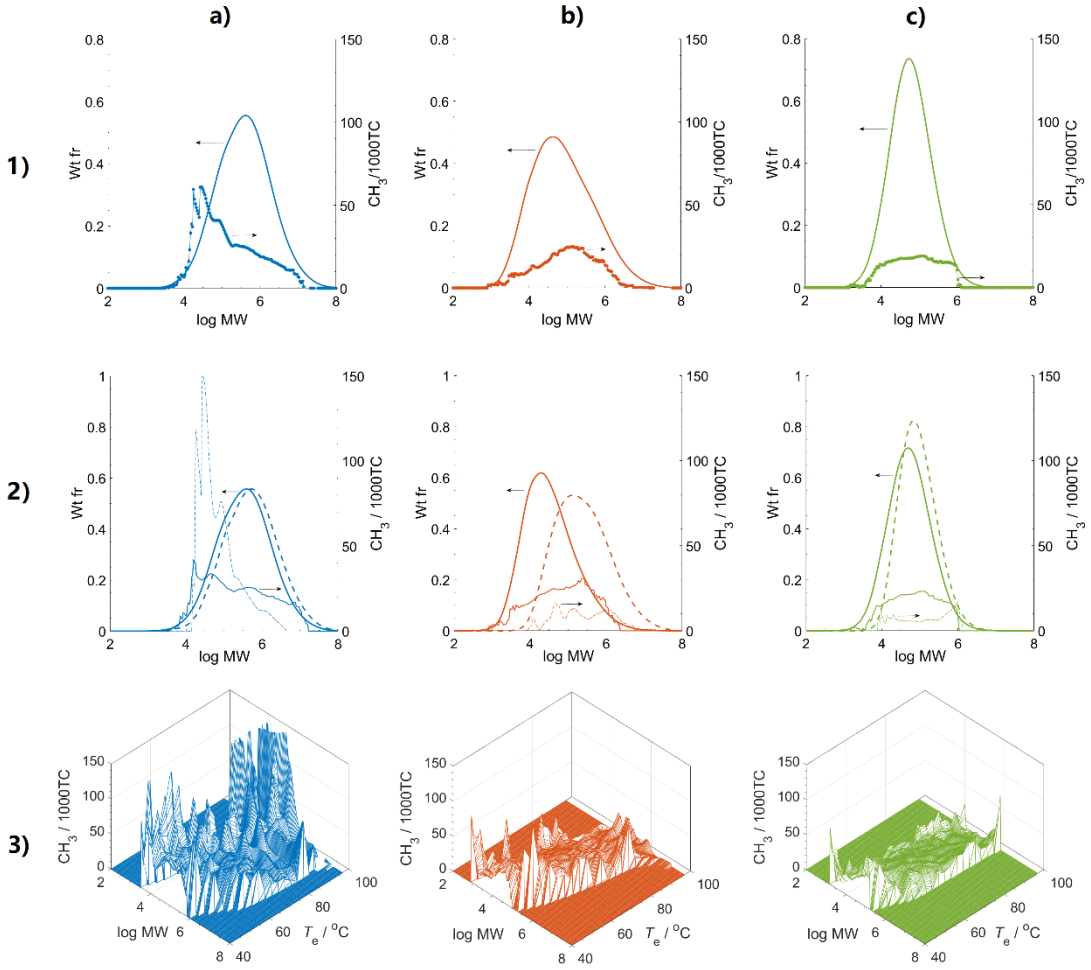

Figure 10 1) GPC-IR data of the crystalline part of the selected samples; 2) GPC-IR data for the $CRYS_{LTe}$ (T_e = 40-85 ℃, solid lines) and $CRYS_{HTe}$ (T_e = 88-97 ℃, dashed lines); 3) CH_3 distribution map of TREF elution fractions (excluding RTSol) measured through CFC (GPC traces are omitted for clarity). 1) and 2) were obtained by summing up the corresponding fractions in 3) in the proportion of weight of each fraction.

Microstructural analysis

Chain ends

^{1}H NMR spectra (Figure 11) of copolymer showed that there are unsaturated chain ends and OH-capped saturated one. The signals are assigned according to literature.[52-54] Typically the unsaturated ones are derived from β-hydrogen transfer/elimination while the saturated one is from transmetalation to alkylaluminum.[77-79] The latter one is minor at low *r*Al,Ti but becomes major at high *r*Al,Ti.

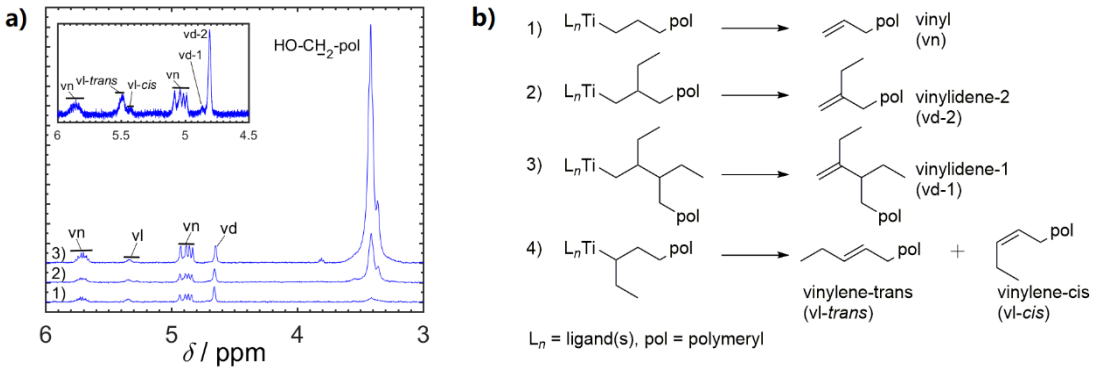

Figure 11. a) ^{1}H NMR spectra of C2/C4 copolymer demonstrate the chain ends, P_{C2}= 4 bar, P_{C4}= 2 bar, P_{H2} = 0.76 bar, TEA as cocatalyst, *r*Al,Ti = **1)** 6, **2)** 12, **3)** 50. Area under curve (total H excluding NMR solvent) was normalized to 1. The inset belongs to a sample with butene incorporation [C4] = 9 mol% at low *r*Al,Ti demonstrating the configurations of vinylene and the types of vinylidene. **b**) The mechanisms generating those chain ends.

The concentration of butene in the gas phase is found to influence the production of butene-derived ends vinylene (vl) and vinylidene (vd) but to hardly affect ethylene-derived end vinyl (vn) as expected (Figure S14). The response pattern of unsaturated ends to alkylaluminum depends on the specific catalyst system. It has been reported that in $Me_2SiCp^*N^tBuZrMe_2$/TIBA/$CPh_3B(C_6F_5)_4$ (Cp* = C_5Me_4)

system vn sharply increases and then slowly decreases while vl and vd decrease over *r*Al,Ti.[80] In (1,2,4-$Me_3Cp)_2ZrCl_2$/MAO/TMA system vd decreases while vn and vl keep constant.[81] In this study all types of unsaturated ends increase over *r*Al,Ti in the absence of H_2 (Table 2). In the presence of H_2, butene-derived ends vl and vd become independent of *r*Al,Ti while ethylene-derived end vn still increases over *r*Al,Ti. The ratio of (vl+vd)/vn declines over *r*Al,Ti and at high *r*Al,Ti becomes similar to C4/C2 in the gas phase (Figure S15).

Table 2. Copolymer microstructure analysis.

Cond[1]	*r*Al,Ti	Olefinic groups[2]			[C4] / mol%	*n*E	*n*B	*r*E	*r*B
		vl	vn	vd					
TEA 20%	3	0.11	0.56	0.25	3.46	33.60	1.00	7.53	0.15
	12	0.12	0.71	0.22	4.56	33.75	1.05	6.44	0.22
	50	0.09	1.20	0.25	3.60	34.27	1.06	7.52	0.25
TEA 33%	3	0.56	0.55	0.33	6.25	16.31	1.05	7.03	0.10
	6	0.11	0.54	0.38	7.42	14.27	1.12	6.65	0.24
	12	0.17	0.69	0.40	8.77	13.67	1.28	6.19	0.58
	24	0.11	1.00	0.37	6.60	16.73	1.20	7.84	0.40
	50	0.14	1.26	0.41	7.47	13.90	1.09	6.59	0.17
TEA 33% without H_2	6	0.07	0.22	0.11	6.56	15.27	1.06	7.04	0.11
	12	0.11	0.43	0.24	7.16	13.55	1.08	6.49	0.16
	24	0.17	0.74	0.26	7.39	14.16	1.12	6.70	0.24
	50	0.18	1.08	0.43	7.71	13.86	1.15	6.31	0.30
TIBA 20%	6	0.40	0.69	0.25	3.56	37.15	1.04	7.79	0.17
	12	0.15	0.68	0.24	4.09	34.72	1.07	7.06	0.32
	50	0.14	1.05	0.24	3.11	38.61	1.05	8.61	0.20
TIBA 33%	12	0.24	0.68	0.36	7.79	14.50	1.19	6.62	0.39
	50	0.21	1.03	0.41	6.27	16.88	1.10	7.78	0.20

[1] Polymerization conditions, cocatalyst, C4 content in gas phase and presence of H_2.
[2] Per 10^4 total carbon (TC).

Sequence analysis

The triads percentage based on ^{13}C NMR is listed in Table S2. And [C4], average sequence length of ethylene *n*E and butene *n*B, apparent reactivity ratio of ethylene (*r*E) and butene (*r*B) are listed in Table 2. Interestingly the reconstructed values from the content of monomeric units of selected triads and tetrads calculated based on first-order Markovian statistics are in good agreement with experimental values despite of the multiple sites nature and blocky characteristics of the polymer (Figure 12).

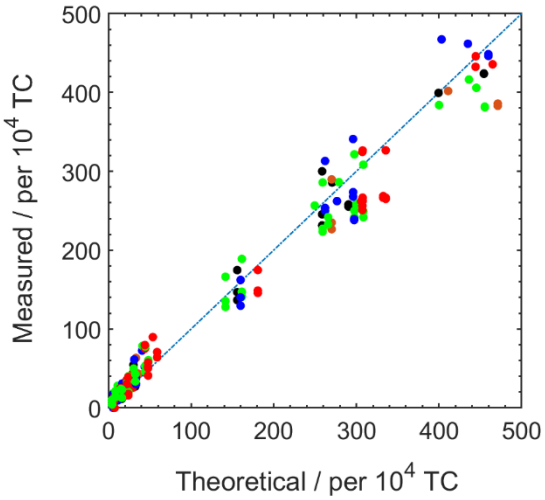

Figure 12. The calculated (theoretically according to first-order Markovian statistics) and measured content of triads and tetrads, including EBE, BBE, EBBE, EBEB, EBEE, BEEB and BEEE of samples prepared in the presence and absence of H_2. *r*Al,Ti = 3 (black), 6 (blue), 12 (red), 24 (brown), 50 (green).

The trend of average length of ethylene sequence *n*E over *r*Al,Ti (Table 2) fails to correlate with the trend of T_m (Table 1). It is particularly clear for the cases without H_2 where *n*E barely changes but T_m significantly grows. It indicates butene units tend to gather together so as to create spaces for long ethylene sequence. Not surprisingly, the apparent reactivity ratio of butene *r*B triples when *r*Al,Ti grows from 6 to 50. And the diads counting deviates from the theoretical value (Figure 13).

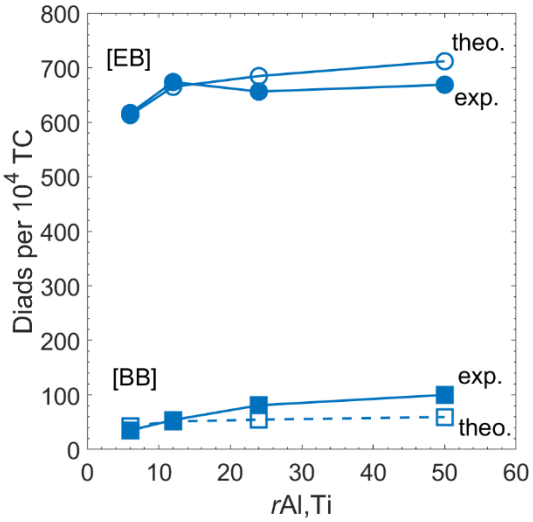

Figure 13. Comparison of the diads (EB and BB) content between the experimental values (full markers) and theoretical values calculated based on first-order Markovian statistics (open markers). Samples were prepared without H_2. P_{C2}= 4 bar, P_{C4}= 2 bar.

A model describing the system

To account for the phenomena aforementioned, herein we propose a model based on the modulation of active species by alkylaluminum (Scheme 1).

The active species A produces statistical copolymer chains. It is susceptible to the effect of alkylaluminum which converts species A into species B producing block chains with C4-enriched segments and C4-scattered segments. If the growing chains of the blocky type are terminated in a right manner, the chunks of the chains can have significant content of butene units. But since the C4-scattered segments are dominant in crystallization process, the chains may still have the same elution temperature as the parent ones have. At low *r*Al,Ti the modulation effect of alkylaluminum is the major one while at high *r*Al,Ti the chain transfer effect prevails. Actually, chain transfer to aluminum leads to low molecular weight C4-rich polymer chains that are soluble at ambient temperature as shown by TREF analysis. There are apparently two families of active species in this system, but they seemingly follow the same principles as proposed.

The exact structure of the active species is unclear yet, but it can be very likely true that the interaction between titanium species and aluminum species is mostly through the Ti-O-Al bridge since OBu group originating from the ingredient $Ti(OBu)_4$ is present in the catalyst as taught by the patent.[47] The complex between alkyl titanates and alkylaluminum has been known for decades.[82-85] The chlorine atoms might play

less important roles in the complexation between Ti and Al in this case, but they are critical for obtaining reasonable activity in olefin polymerization possibly due to electronic effects.[86-88] On the other hand, in the cases involving chlorinated derivatives of alkylaluminum,[32, 34-37] the Ti-Cl-Al bonding may need to be considered regarding the coordinative capability of them[24-25, 89-90].

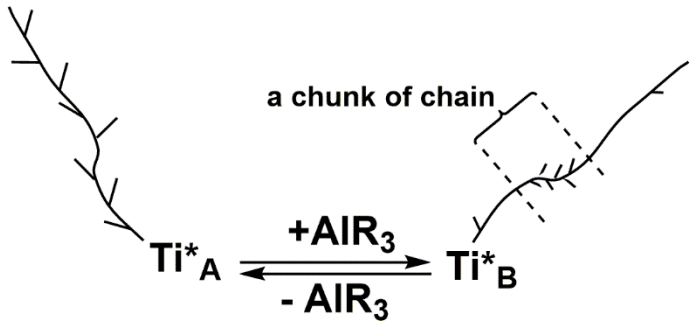

Scheme 1. Schematic mechanisms of polymerization involving the participation of AlR_3. The chunk of chain containing C4-rich segment may cause significantly high CH_3 counting if being cut off during chain growth.

About block copolymer of Ziegler-Natta-type systems

Currently commercial olefin block copolymers (OBCs) are produced with molecular catalysts through chain shuttling process, e.g. INFUSE™ and INTUNE™ of Dow Chemical.[91-93] However the existence of blocky structures (stereoblocks) in polypropylene produced with Ziegler-Natta catalysts have been debated about for decades.[20, 94] Recently De Rosa et al. through analyzing the crystallization behaviors proposed the existence of blocky structures in poly(1-butene-*co*-ethylene) produced by a classic fourth-generation ZNC.[95-96] It is hard to conclude how common block copolymer is due to clear differences between the preparation procedures of ZNCs.

However, it could be worthwhile to investigate this topic given the importance of blocky structures to property improvement of the material.[97]

CONCLUSIONS

A novel $SiO_2/MgCl_2$-bisupported catalyst has been studied in gas phase ethylene/1-butene copolymerization. It has been concluded that:

i. AlR_3 is required with minimal amount to activate the catalyst. However, high dosage of AlR_3 up to 7.2 mmol retards the catalyst without killing it.

ii. Adjusting the dosage of AlR_3 impacts the chemical composition of the produced copolymers. Blocky characteristics of the copolymer are demonstrated at low *r*Al,Ti but fade at high *r*Al,Ti. Higher dosage of alkylaluminum also gives rise to longer ethylene sequences along with increasing butene sequences so that the overall comonomer incorporation is not significantly impacted.

iii. It is proposed that active species can be modified by alkylaluminum to produce copolymer segments with different chemical composition. Block copolymer chains can be produced upon the reversible coordination of alkylaluminum to the active species. The blocky characteristics are reduced by chain transfer reaction through interrupting the growth of the block chains.

This fundamental study permits to conclude that in spite of a similar butene content in copolymer obtained at various dosages of alkylaluminum, low *r*Al,Ti should be

preferred in terms of limiting soluble fraction and of promoting blocky characteristics of copolymer.

AUTHOR INFORMATION

Corresponding Authors

*E-mail: christophe.boisson@univ-lyon1.fr (C. Boisson)

*E-mail: marcia.miranda@braskem.com (M. Miranda)

ORCID

Yue Yu: 0000-0002-7520-0547

Timothy F. L. McKenna: 0000-0001-6437-5942

Christophe Boisson: 0000-0002-7909-901X

Author Contributions

The manuscript was written through contributions of all authors. All authors have given approval to the final version of the manuscript.

Funding Sources

ASSOCIATED CONTENT #This paragraph has been moved from other position to here#

Supporting Information.

This information is available free of charge on the ACS Publications website.

DSC and GPC profiles of the samples, CEF and TGIC profiles of the samples and a comparative sample made with classic ZNC, ^{13}C NMR spectrum of *n*-pentane soluble

fraction, GPC data of CFC fractions, dependence of unsaturated chain ends on *r*Al,Ti, triads content of the samples.

ACKNOWLEDGMENT

Braskem SA is acknowledged for scientific and financial support of this project. The authors would like to thank Mr. Olivier Boyron (LCPP@C2P2) and Ms. Manel Taam (LCPP@C2P2) for help with the CEF and TGIC analysis. The authors appreciate the CFC analysis of Polymer Char. And the authors are indebted to Prof. João B. P. Soares (University of Alberta) for the GPC-IR analysis.

REFERENCES

1. Bochmann, M.; Lancaster, S. J. Monomer–dimer equilibria in homo- and heterodinuclear cationic alkylzirconium complexes and their role in polymerization catalysis. *Angew. Chem. Int. Ed.* **1994,** 33, 1634-1637.
2. Babushkin, D. E.; Semikolenova, N. V.; Zakharov, V. A.; Talsi, E. P. Mechanism of dimethylzirconocene activation with methylaluminoxane: NMR monitoring of intermediates at high Al/Zr ratios. *Macromol. Chem. Phys.* **2000,** 201, 558-567.
3. Bolton, P. D.; Clot, E.; Cowley, A. R.; Mountford, P. Well-defined imidotitanium alkyl cations: agostic interactions, migratory insertion vs. [2+2] cycloaddition, and the first structurally authenticated AlMe3 adduct of any transition metal alkyl cation. *Chem. Commun.* **2005**, 3313-3315.
4. Bolton, P. D.; Clot, E.; Cowley, A. R.; Mountford, P. $AlMe_3$ and $ZnMe_2$ adducts of a titanium imido methyl cation: A combined crystallographic, spectroscopic, and DFT study. *J. Am. Chem. Soc.* **2006,** 128, 15005-15018.
5. Babushkin, D. E.; Brintzinger, H. H. Modification of methylaluminoxane-activated *ansa*-zirconocene catalysts with triisobutylaluminum—transformations of reactive cations studied by NMR spectroscopy. *Chem. Eur. J.* **2007,** 13, 5294-5299.
6. Korobkov, I.; Gambarotta, S. Aluminate samarium(II) and samarium(III) aryloxides. Isolation of a single-component ethylene polymerization catalyst. *Organometallics* **2009,** 28, 4009-4019.
7. Gurubasavaraj, P. M.; Nomura, K. Hetero-bimetallic complexes of titanatranes with aluminum alkyls: Synthesis, structural analysis, and their use in catalysis for ethylene polymerization. *Organometallics* **2010,** 29, 3500-3506.
8. Baldwin, S. M.; Bercaw, J. E.; Brintzinger, H. H. Cationic alkylaluminum-complexed zirconocene hydrides as participants in olefin polymerization catalysis. *J. Am. Chem. Soc.* **2010,** 132, 13969-13971.
9. Camara, J. M.; Petros, R. A.; Norton, J. R. Zirconium-catalyzed carboalumination of α-olefins and chain growth of aluminum alkyls: Kinetics and mechanism. *J. Am. Chem. Soc.* **2011,** 133, 5263-5273.
10. Lenton, T. N.; Bercaw, J. E.; Panchenko, V. N.; Zakharov, V. A.; Babushkin, D. E.; Soshnikov, I. E.; Talsi, E. P.; Brintzinger, H. H. Formation of trivalent zirconocene complexes from *ansa*-zirconocene-based olefin-polymerization precatalysts: An EPR- and NMR-spectroscopic study. *J. Am. Chem. Soc.* **2013,** 135, 10710-10719.
11. Theurkauff, G.; Bondon, A.; Dorcet, V.; Carpentier, J.-F.; Kirillov, E. Heterobi- and -trimetallic ion pairs of zirconocene-based isoselective olefin polymerization catalysts with $AlMe_3$. *Angew. Chem. Int. Ed.* **2015,** 54, 6343-6346.
12. Ehm, C.; Cipullo, R.; Budzelaar, P. H. M.; Busico, V. Role(s) of TMA in polymerization. *Dalton Trans.* **2016,** 45, 6847-6855.
13. Cossee, P. Stereoregularity in heterogeneous Ziegler-Natta catalysis. *Trans. Faraday Soc.* **1962,** 58, 1226-1232.
14. Rodriguez, L. A.; van Looy, H. M. Studies on Ziegler-Natta catalysts .V. Stereospecificity of active center. *J. Polym. Sci. A Polym. Chem.* **1966,** 4, 1971-1992.

15. Corradini, P.; Barone, V.; Fusco, R.; Guerra, G. A possible model of catalytic sites for the stereospecific polymerization of alpha-olefins on 1st-generation and supported Ziegler-Natta catalysts. *Gazz. Chim. Ital.* **1983,** 113, 601-607.
16. Corradini, P.; Guerra, G.; Cavallo, L. Do new century catalysts unravel the mechanism of stereocontrol of old Ziegler-Natta catalysts? *Acc. Chem. Res.* **2004,** 37, 231-241.
17. Busico, V.; Cipullo, R.; Monaco, G.; Talarico, G.; Vacatello, M.; Chadwick, J. C.; Segre, A. L.; Sudmeijer, O. High-resolution ^{13}C NMR configurational analysis of polypropylene made with $MgCl_2$-supported Ziegler-Natta catalysts. 1. The "model" system $MgCl_2/TiCl_4$-2,6-dimethylpyridine/$Al(C_2H_5)_3$. *Macromolecules* **1999,** 32, 4173-4182.
18. Sacchi, M. C.; Forlini, F.; Tritto, I.; Locatelli, P.; Morini, G. A study for distinguishing mono- and bimetallic mechanisms in heterogeneous Ziegler-Natta catalysis. *Macromol. Chem. Phys.* **1995,** 196, 2881-2890.
19. Kohara, T.; Shinoyama, M.; Doi, Y.; Keii, T. Elimination and replacement of organometallic co-catalysts during polymerization of propene with heterogeneous Ziegler-Natta catalysts. *Macromol. Chem.* **1979,** 180, 2139-2151.
20. Doi, Y. Structure and stereochemistry of atactic polypropylenes. Statistical model of chain propagation. *Makromol. Chem. Rapid Commun.* **1982,** 3, 635-641.
21. Xu, J.; Feng, L.; Yang, S. Formation mechanism of stereoblocks in polypropylene produced by supported Ziegler−Natta catalysts. *Macromolecules* **1997,** 30, 2539-2541.
22. Liu, B. P.; Nitta, T.; Nakatani, H.; Terano, M. Specific roles of Al-alkyl cocatalyst in the origin of isospecificity of active sites on donor-free $TiCl_4/MgCl_2$ Ziegler-Natta catalyst. *Macromol. Chem. Phys.* **2002,** 203, 2412-2421.
23. Blaakmeer, E. S.; van Eck, E. R. H.; Kentgens, A. P. M. The coordinative state of aluminium alkyls in Ziegler-Natta catalysts. *Phys. Chem. Chem. Phys.* **2018,** 20, 7974-7988.
24. Potapov, A. G.; Terskikh, V. V.; Zakharov, V. A.; Bukatov, G. D. ^{27}Al NMR MAS study of the surface Al complexes formed in reaction of organoaluminium compounds with supported $TiCl_4/MgCl_2$ catalyst. *J. Mol. Catal. A Chem.* **1999,** 145, 147-152.
25. Vittoria, A.; Meppelder, A.; Friederichs, N.; Busico, V.; Cipullo, R. Demystifying Ziegler–Natta catalysts: The origin of stereoselectivity. *ACS Catal.* **2017**, 4509-4518.
26. Morra, E.; Giamello, E.; Van Doorslaer, S.; Antinucci, G.; D'Amore, M.; Busico, V.; Chiesa, M. Probing the coordinative unsaturation and local environment of Ti^{3+} sites in an activated high-yield Ziegler-Natta catalyst. *Angew. Chem. Int. Edit.* **2015,** 54, 4857-4860.
27. Piovano, A.; Thushara, K. S.; Morra, E.; Chiesa, M.; Groppo, E. Unraveling the catalytic synergy between Ti^{3+} and Al^{3+} sites on a chlorinated Al_2O_3: A tandem approach to branched polyethylene. *Angew. Chem. Int. Edit.* **2016,** 55, 11203-11206.
28. Shan, C. L. P.; Chu, K.-J.; Soares, J.; Penlidis, A. Using alkylaluminium activators to tailor short chain branching distributions of ethylene/1-hexene copolymers produced with in-situ supported metallocene catalysts. *Macromol. Chem. Phys.* **2000,** 201, 2195-2202.

29. Wang, W.; Nomura, K. Notable effects of aluminum alkyls and solvents for highly efficient ethylene (co)polymerizations catalyzed by (arylimido)-(aryloxo)vanadium complexes. *Adv. Synth. Catal.* **2006,** 348, 743-750.
30. Guo, Y.; Fu, Z.; Xu, J.; Fan, Z. Structure and properties of ethylene/propylene copolymers synthesized with bis(2,4,7-trimethylindenyl)zirconium dichloride activated by methyl aluminoxanes containing different amount of trimethylaluminum. *Polymer* **2017,** 122, 77-86.
31. Fryga, J.; Białek, M. Effect of AlR_3 (R = Me, Et, *i*Bu) addition on the composition and microstructure of ethylene/1-olefin copolymers made with post-metallocene complexes of group 4 elements. *Polym. J.* **2019**, 51, 19-29.
32. Yoon, J.-S.; Jeung, Y.-T.; Park, J.-W.; Kim, J.-Y.; Lee, D.-H. Studies on the catalyst modification in propylene polymerization using ethylene-propylene copolymerization. *Polym. Bull.* **1989,** 22, 233-238.
33. Koivumäki, J.; Seppälä, J. V.; Kuutti, L. Effect of the cocatalyst on the copolymerization of ethylene and propylene with high activity Ziegler-Natta catalyst. *Polym. Bull.* **1992,** 29, 185-191.
34. Chu, K.-J.; Soares, J. B. P.; Penlidis, A.; Ihm, S.-K. Effect of prepolymerization and hydrogen pressure on the microstructure of ethylene/1-hexene copolymers made with $MgCl_2$-supported $TiCl_3$ catalysts. *Eur. Polym. J.* **2000,** 36, 3-11.
35. Chen, Y.-p.; Fan, Z.-q. Ethylene/1-hexene copolymerization with $TiCl_4/MgCl_2/AlCl_3$ catalyst in the presence of hydrogen. *Eur. Polym. J.* **2006,** 42, 2441-2449.
36. Garroff, T.; Waldvogel, P.; Kalle, K.; Eriksson, V.; Aittola, A.; Kokko, E. Linear low density polyethylene with uniform or reversed comonomer composition distribution. US Patent 8546499B2, 2013.
37. Aigner, P.; Averina, E.; Garoff, T.; Paulik, C. Effects of alterations to Ziegler–Natta catalysts on kinetics and comonomer (1- butene) incorporation. *Macromol. React. Eng.* **2017,** 11, 1700009.
38. Chen, K.; Mehdiabadi, S.; Liu, B.; Soares, J. B. P. Analysis of ethylene/1-olefin copolymers made with Ziegler–Natta catalysts by deconvolution of molecular weight and average short chain branching distributions. *Macromol. React. Eng.* **2016,** 10, 206-214.
39. Soares, J. B. P. An overview of important microstructural distributions for polyolefin analysis. *Macromol. Symp.* **2007,** 257, 1-12.
40. Soares, J. B. P.; McKenna, T. F. L. Polyolefin Microstructural Modeling. In *Polyolefin Reaction Engineering;* Wiley- VCH Verlag GmbH & Co. KGaA: Weinheim, 2012; pp 187-269.
41. Scheirs, J.; Böhm, L. L.; Boot, J. C.; Leevers, P. S. PE100 resins for pipe applications: Continuing the development into the 21st century. *Trends Polym. Sci.* **1996,** 4, 408-415.
42. Alt, F. P.; Böhm, L. L.; Enderle, H.-F.; Berthold, J. Bimodal polyethylene – Interplay of catalyst and process. *Macromol. Symp.* **2001,** 163, 135-144.
43. Follestad, A.; Ommundsen, E. Improvements in or relating to polymers. WO2001009200A1, 2001.

44. Liu, H.-T.; Davey, C. R.; Shirodkar, P. P. Bimodal polyethylene products from UNIPOL^{TM} single gas phase reactor using engineered catalysts. *Macromol. Symp.* **2003,** 195, 309-316.
45. DesLauriers, P. J.; McDaniel, M. P.; Rohlfing, D. C.; Krishnaswamy, R. K.; Secora, S. J.; Benham, E. A.; Maeger, P. L.; Wolfe, A. R.; Sukhadia, A. M.; Beaulieu, B. B. A comparative study of multimodal vs. bimodal polyethylene pipe resins for PE-100 applications. *Polym. Eng. Sci.* **2005,** 45, 1203-1213.
46. Paulik, C.; Spiegel, G.; Jeremic, D. Bimodal Polyethylene: Controlling Polymer Properties by Molecular Design. In *Multimodal Polymers with Supported Catalysts: Design and Production;* Albunia, A. R., Prades, F., Jeremic, D., Eds; Springer International Publishing: Cham, 2019; pp 243-265.
47. Amorim, R. F.; Braganca, A. L. D.; Dos Santos Silveira, L.; Miranda, M. S. L. Solid catalyst component for polymerization and copolymerization of ethylene, and, process for obtaining the same. European Patent 1515995B1, 2010.
48. Müller, A. J.; Hernández, Z. H.; Arnal, M. L.; Sánchez, J. J. Successive self-nucleation/annealing (SSA): A novel technique to study molecular segregation during crystallization. *Polym. Bull.* **1997,** 39, 465-472.
49. Arnal, M. L.; Balsamo, V.; Ronca, G.; Sánchez, A.; Müller, A. J.; Cañizales, E.; Urbina de Navarro, C. Applications of successive self-nucleation and annealing (SSA) to polymer characterization. *J. Therm. Anal. Calorim.* **2000,** 59, 451-470.
50. Müller, A. J.; Michell, R. M.; Pérez, R. A.; Lorenzo, A. T. Successive Self-nucleation and Annealing (SSA): Correct design of thermal protocol and applications. *Eur. Polym. J.* **2015,** 65, 132-154.
51. Ortin, A.; Monrabal, B.; Sancho-Tello, J. Development of an automated cross-fractionation apparatus (TREF-GPC) for a full characterization of the bivariate distribution of polyolefins. *Macromol. Symp.* **2007,** 257, 13-28.
52. Rossi, A.; Zhang, J. B.; Odian, G. Microstructure of ethylene-1-butene copolymers produced by zirconocene methylaluminoxane catalysis. *Macromolecules* **1996,** 29, 2331-2338.
53. He, Y. Y.; Qiu, X. H.; Klosin, J.; Cong, R. J.; Roof, G. R.; Redwine, D. Terminal and internal unsaturations in poly(ethylene-*co*-1-octene). *Macromolecules* **2014,** 47, 3782-3790.
54. Busico, V.; Cipullo, R.; Friederichs, N.; Linssen, H.; Segre, A.; Van Axel Castelli, V.; van der Velden, G. ^{1}H NMR analysis of chain unsaturations in ethene/1-octene copolymers prepared with metallocene catalysts at high temperature. *Macromolecules* **2005,** 38, 6988-6996.
55. Randall, J. C. A review of high resolution liquid ^{13}carbon nuclear magnetic resonance characterizations of ethylene-based polymers. *J. Macromol. Sci. C* **1989,** 29, 201-317.
56. Kim, I.; Kim, J. H.; Woo, S. I. Kinetic study of ethylene polymerization by highly active silica supported $TiCl_4/MgCl_2$ catalysts. *J. Appl. Polym. Sci.* **1990,** 39, 837-854.
57. Han-Adebekun, G. C.; Hamba, M.; Ray, W. H. Kinetic study of gas phase olefin polymerization with a $TiCl_4/MgCl_2$ catalyst I. Effect of polymerization conditions. *J. Polym. Sci. A Polym. Chem.* **1997,** 35, 2063-2074.

58. Trischler, H.; Hochfurtner, T.; Ruff, M.; Paulik, C. Influence of the aluminum alkyl co-catalyst type in Ziegler-Natta ethene polymerization on the formation of active sites, polymerization rate, and molecular weight. *Kinet. Catal.* **2013,** 54, 559-565.
59. Rieger, B.; Janiak, C. Concentration effects of methylalumoxane, zirconocene dichloride and trimethylaluminum in ethylene polymerization. *Angew. Makromol. Chem.* **1994,** 215, 35-46.
60. Michiels, W.; Muñoz-Escalona, A. Mixed cocatalyst systems in metallocene ethylene polymerization. *Macromol. Symp.* **1995,** 97, 171-183.
61. Hammawa, H.; Mannan, T. M.; Lynch, D. T.; Wanke, S. E. Effects of aluminum alkyls on ethylene/1-hexene polymerization with supported metallocene/MAO catalysts in the gas phase. *J. Appl. Polym. Sci.* **2004,** 92, 3549-3560.
62. Müller, A. J.; Arnal, M. L. Thermal fractionation of polymers. *Prog. Polym. Sci.* **2005,** 30, 559-603.
63. Fillon, B.; Wittmann, J. C.; Lotz, B.; Thierry, A. Self-nucleation and recrystallization of isotactic polypropylene (α phase) investigated by differential scanning calorimetry. *J. Polym. Sci. B* **1993,** 31, 1383-1393.
64. Porcello, J. M. B.; Cardozo, N. S. M.; Forte, M. M. C.; Wolf, C. R.; de Camargo, M. Linear low-density polyethylene softening point and endothermic curve profile correlation: DSC technique. *Int. J. Polym. Anal. Charact.* **2011,** 16, 95-106.
65. Cho, T. Y.; Heck, B.; Strobl, G. Equations describing lamellar structure parameters and melting points of polyethylene-co-(butene/octene)s. *Colloid. Polym. Sci.* **2004,** 282, 825-832.
66. Monrabal, B.; Romero, L.; Mayo, N.; Sancho-Tello, J. Advances in crystallization elution fractionation. *Macromol. Symp.* **2009,** 282, 14-24.
67. Monrabal, B.; Sancho-Tello, J.; Mayo, N.; Romero, L. Crystallization elution fractionation. A new separation process for polyolefin resins. *Macromol. Symp.* **2007,** 257, 71-79.
68. Beigzadeh, D.; Soares, J. B. P.; Duever, T. A. Modeling of fractionation in CRYSTAF using Monte Carlo simulation of crystallizable sequence lengths: Ethylene/1-octene copolymers synthesized with single-site–type catalysts. *J. Appl. Polym. Sci.* **2001,** 80, 2200-2206.
69. Cong, R.; deGroot, W.; Parrott, A.; Yau, W.; Hazlitt, L.; Brown, R.; Miller, M.; Zhou, Z. A new technique for characterizing comonomer distribution in polyolefins: High-temperature thermal gradient interaction chromatography (HT-TGIC). *Macromolecules* **2011,** 44, 3062-3072.
70. Cong, R.; deGroot, A. W.; Parrott, A.; Yau, W.; Hazlitt, L.; Brown, R.; Cheatham, M.; Miller, M. D.; Zhou, Z. High temperature thermal gradient interaction chromatography (HT-TGIC) for microstructure analysis of polyolefins. *Macromol. Symp.* **2012,** 312, 108-114.
71. Pasch, H.; Malik, M. I.; Macko, T. Recent Advances in High-Temperature Fractionation of Polyolefins. In *Polymer Composites – Polyolefin Fractionation – Polymeric Peptidomimetics – Collagens;* Abe, A., Kausch, H.-H., Möller, M., Pasch, H., Eds; Springer Berlin Heidelberg: Berlin, Heidelberg, 2013; pp 77-140.

72. Monrabal, B.; López, E.; Romero, L. Advances in thermal gradient interaction chromatography and crystallization techniques for composition analysis in polyolefins. *Macromol. Symp.* **2013,** 330, 9-21.
73. Monrabal, B.; Romero, L. Separation of polypropylene polymers by crystallization and adsorption techniques. *Macromol. Chem. Phys.* **2014,** 215, 1818-1828.
74. Zhou, Z.; Miller, M. D.; Lee, D.; Cong, R.; Klinker, C.; Huang, T.; Li Pi Shan, C.; Winniford, B.; deGroot, A. W.; Fan, L.; Karjala, T.; Beshah, K. NMR study of the separation mechanism of polyethylene–octene block copolymer by HT-LC with graphite. *Macromolecules* **2015,** 48, 7727-7732.
75. Kot, D.; Macko, T.; Arndt, J.-H.; Brüll, R. Porous graphite as platform for the separation and characterization of synthetic polymers – an overview. *J Chromatogr A* **2019,** 1606, 360038.
76. Al-Khazaal, A. Z.; Soares, J. B. P. Joint effect of poly(ethyhlene-co-1-octene) chain length and 1-octene fraction on high-temperature thermal gradient interaction chromatography. *Macromol. Chem. Phys.* **2017,** 218, 1600332.
77. Yu, Y.; Fu, Z. S.; Fan, Z. Q. Chain transfer reactions of propylene polymerization catalyzed by $AlEt_3$ activated $TiCl_4/MgCl_2$ catalyst under very low monomer addition rate. *J. Mol. Catal. A Chem.* **2012,** 363, 134-139.
78. Resconi, L.; Camurati, I.; Sudmeijer, O. Chain transfer reactions in propylene polymerization with zirconocene catalysts. *Top. Catal.* **1999,** 7, 145-163.
79. Kang, K. K.; Shiono, T.; Ikeda, T. Synthesis of aluminum-terminated polypropylene by a $MgCl_2$-supported $TiCl_4$ catalyst combined with Al(*i*-Bu)$_3$ as cocatalyst. *Macromolecules* **1997,** 30, 1231-1233.
80. Panin, A. N.; Sukhova, T. A.; Bravaya, N. M. Triisobutylaluminum as cocatalyst for zirconocenes. I. Sterically opened zirconocene/triisobutylaluminum/perfluorophenylborate as highly effective ternary catalytic system for synthesis of low molecular weight polyethylenes. *J. Polym. Sci. A Polym. Chem.* **2001,** 39, 1901-1914.
81. Bruaseth, I.; Bahr, M.; Gerhard, D.; Rytter, E. Pressure and trimethylaluminum effects on ethene/1-hexene copolymerization with methylaluminoxane-activated (1,2,4-$Me_3Cp)_2ZrCl_2$: Trimethylaluminum suppression of standard termination reactions after 1-hexene insertion. *J. Polym. Sci. A Polym. Chem.* **2005,** 43, 2584-2597.
82. Woo, T. W.; Woo, S. I. Kinetic study of ethylene dimerization catalyzed over Ti(O-*n*$C_4H_9)_4/AlEt_3$. *J. Catal.* **1991,** 132, 68-78.
83. Hirai, H.; Hiraki, K.; Noguchi, I.; Makishima, S. Electron spin resonance study on homogeneous catalysts derived from *n*-butyl titanate and triethylaluminum. *J. Polym. Sci. A Polym. Chem.* **1970,** 8, 147-156.
84. Yamazaki, N.; Takeuchi, H.; Hino, S.; Shu, T.; Deshpande, A. B. Investigation of catalyst systems containing titanium-*n*-tetrabutoxide and aluminium alkyls. *J. Polym. Sci. A Polym. Chem.* **1972,** 10, 309-313.
85. Robinson, R.; McGuinness, D. S.; Yates, B. F. The mechanism of ethylene dimerization with the Ti(OR')$_4$/AlR_3 catalytic system: DFT studies comparing

metallacycle and Cossee proposals. *ACS Catal.* **2013,** 3, 3006-3015.
86. Zucchini, U.; Cuffiani, I.; Pennini, G. Ethylene polymerization by high yield co-milled catalysts, 1. Influence of titanium ligands on the activity of the catalyst. **1984,** 5, 567-571.
87. Zhang, Q.; Wang, H.; Gao, K. Study on the gas-phase homopolymerization and copolymerization of olefine with double component $TiOBu_4/TiCl_4$ supported catalysts. *Polym. Mater. Sci. Eng.* **2002,** 18, 94-97.
88. Gao, K.; Wang, H.; Zhang, Q.; An, J.; Lu, X. Study on Z-N catalyst for LLDPE synthesis through gas-phase polymerization. *Petrochem. Technol.* **2003,** 32, 658-662.
89. Potapov, A. G.; Terskikh, V. V.; Bukatov, G. D.; Zakharov, V. A. ^{27}Al MAS NMR study of the interaction of supported Ziegler–Natta catalysts with organoaluminium co-catalyst in the presence of donors. *J. Mol. Catal. A Chem.* **2000,** 158, 457-460.
90. Potapov, A. G.; Terskikh, V. V.; Bukatov, G. D.; Zakharov, V. A. ^{27}Al NMR MAS study of $AlEt_{3-n}Cl_n/MgCl_2$ systems. *J. Mol. Catal. A Chem.* **1997,** 122, 61-65.
91. Hustad, P. D.; Kuhlman, R. L.; Arriola, D. J.; Carnahan, E. M.; Wenzel, T. T. Continuous Production of Ethylene-Based Diblock Copolymers Using Coordinative Chain Transfer Polymerization. *Macromolecules* **2007,** 40, 7061-7064.
92. Arriola, D. J.; Carnahan, E. M.; Hustad, P. D.; Kuhlman, R. L.; Wenzel, T. T. Catalytic production of olefin block copolymers via chain shuttling polymerization. *Science* **2006,** 312, 714-719.
93. Wenzel, T. T.; Arriola, D. J.; Carnahan, E. M.; Hustad, P. D.; Kuhlman, R. L. Chain Shuttling Catalysis and Olefin Block Copolymers (OBCs). In *Metal Catalysts in Olefin Polymerization;* Guan, Z., Ed. Springer Berlin Heidelberg: Berlin, Heidelberg, 2009; pp 65-104.
94. Busico, V.; Cipullo, R.; Corradini, P.; De Biasio, R. Propene polymerization in the presence of $MgCl_2$-supported Ziegler-Natta catalysts, 5. Microstructural characterization of the "isotactic" (heptane-insoluble) polypropene fractions. *Macromol. Chem. Phys.* **1995,** 196, 491-498.
95. De Rosa, C.; Ruiz de Ballesteros, O.; Auriemma, F.; Talarico, G.; Scoti, M.; Di Girolamo, R.; Malafronte, A.; Piemontesi, F.; Liguori, D.; Camurati, I.; Morini, G. Crystallization Behavior of Copolymers of Isotactic Poly(1-butene) with Ethylene from Ziegler–Natta Catalyst: Evidence of the Blocky Molecular Structure. *Macromolecules* **2019,** 52, 9114-9127.
96. De Rosa, C.; Ruiz de Ballesteros, O.; Di Girolamo, R.; Malafronte, A.; Auriemma, F.; Talarico, G.; Scoti, M. The blocky structure of Ziegler–Natta "random" copolymers: myths and experimental evidence. *Polym. Chem.* **2020,** 11, 34-38.
97. Eagan, J. M.; Xu, J.; Di Girolamo, R.; Thurber, C. M.; Macosko, C. W.; LaPointe, A. M.; Bates, F. S.; Coates, G. W. Combining polyethylene and polypropylene: Enhanced performance with PE/iPP multiblock polymers. *Science* **2017,** 355, 814-816.

BRIEFS

Alkylaluminum is proposed to modify the active species to produce different polyolefin blocks and to tune the copolymer chains between statistical ones and block ones.

SYNOPSIS

#TOC figure has been updated#